Supplementary Information

Structure-directing synthesis of porous $CuO–SiO_2$ nanocomposites using carbon nitride

Yuki Takeuchi,[a] Yasuhiro Toyoda,[b] Kazuma Gotoh[b] and Takahiro Ohkubo*[a]

[a] Graduate School of Natural Science and Technology, Okayama University, 3-1-1 Tsushimanaka, Kita-ku, Okayama 700-8530, Japan

[b] Center for Nano Materials and Technology, Japan Advanced Institute of Science and Technology (JAIST), 1-1 Asahidai, Nomi, Ishikawa, 923-1292, Japan

Figure and table

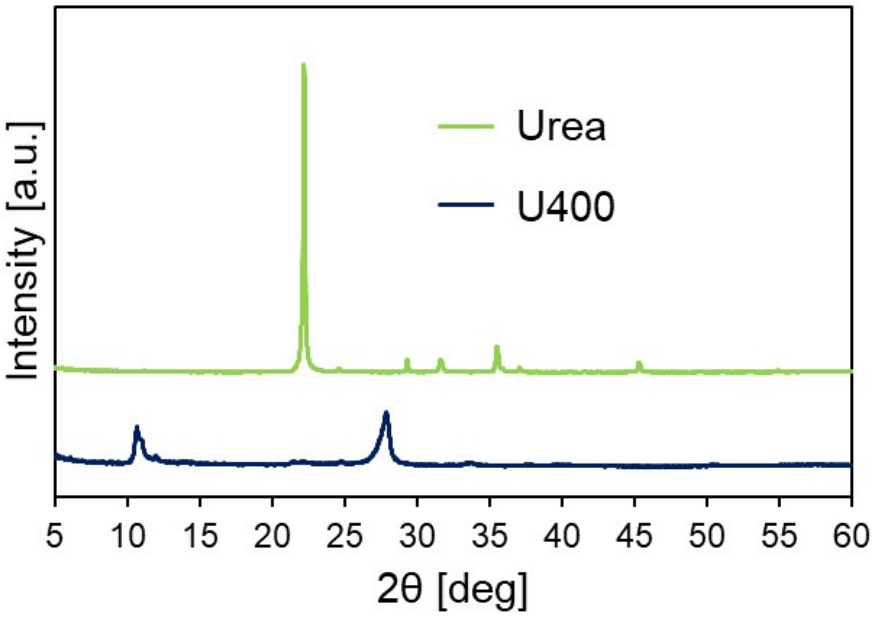

Fig. S1 XRD patterns for urea and U400.

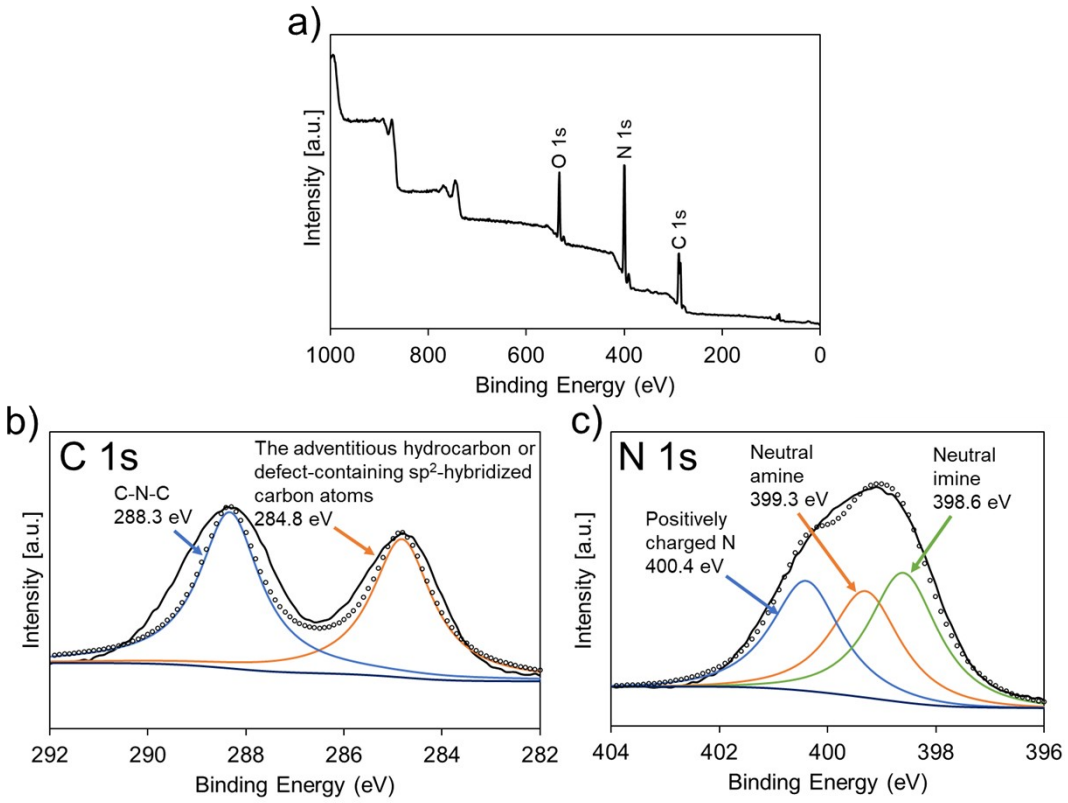

Fig. S2 a) XPS survey scan, and high-resolution XPS spectra in b) C 1s region and c) N 1s region for U400.

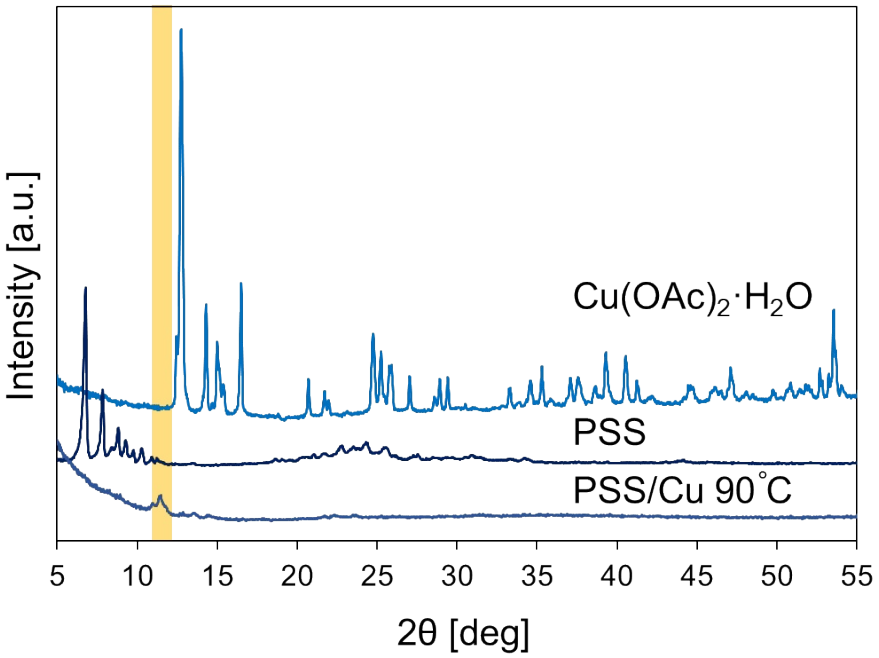

Fig. S3 XRD patterns for $Cu(OAc)_2 \cdot H_2O$, PSS, and PSS/Cu 90°C.

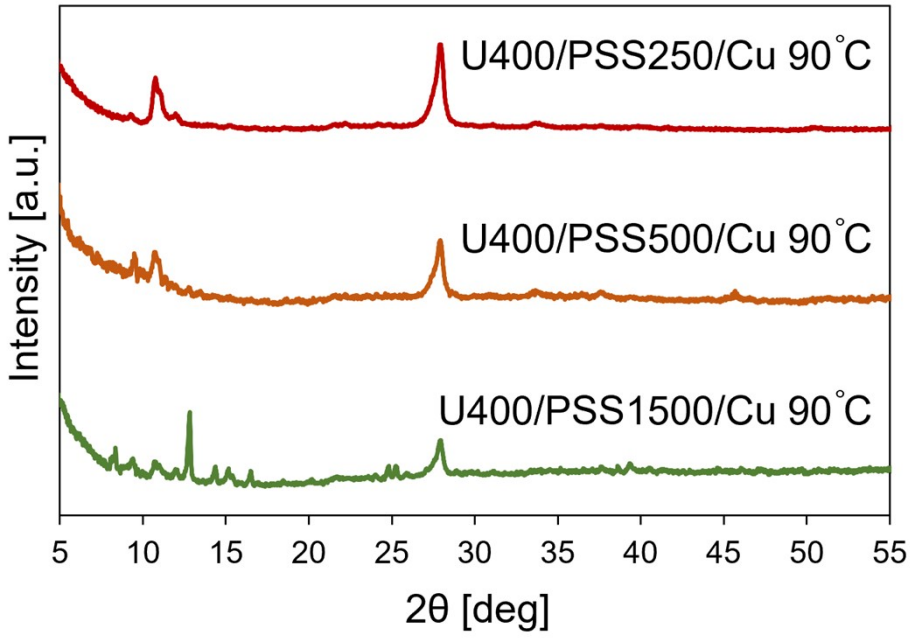

Fig. S4 XRD patterns for each U400/PSSx/Cu 90°C.

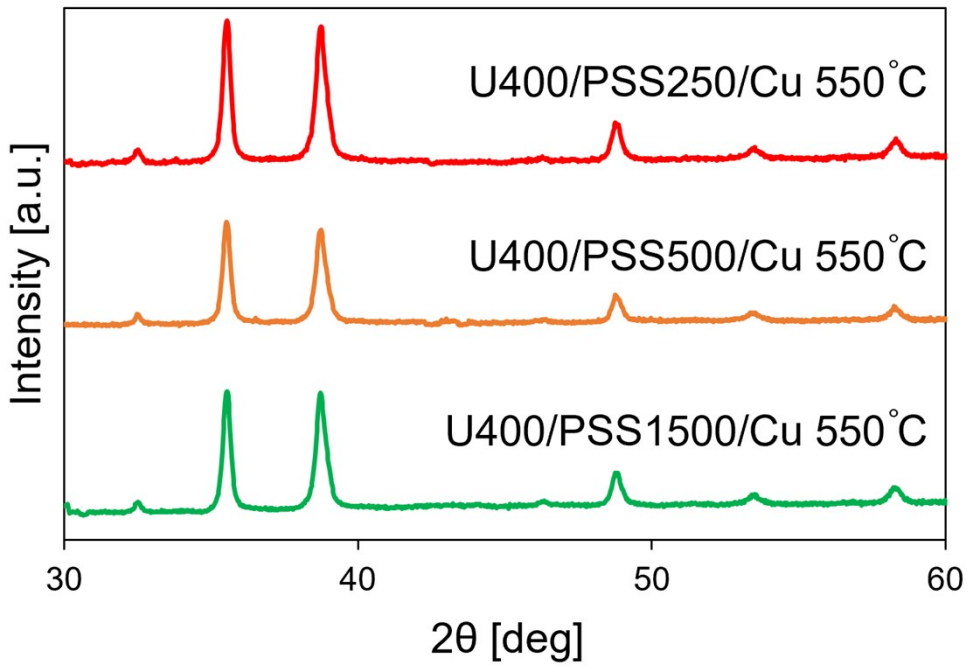

Fig. S5 XRD patterns for each U400/PSSx/Cu 550°C.

Table S1 Widths at half-maximum intensity of each peak in U400/PSS250/Cu 550°C and $Cu(OAc)_2 \cdot H_2O$ 550°C.

	The peak at 2θ = 36° [°]	The peak at 2θ = 39° [°]
U400/PSS250/Cu 550°C	0.32	0.41
$Cu(OAc)_2 \cdot H_2O$ 550°C	0.29	0.31

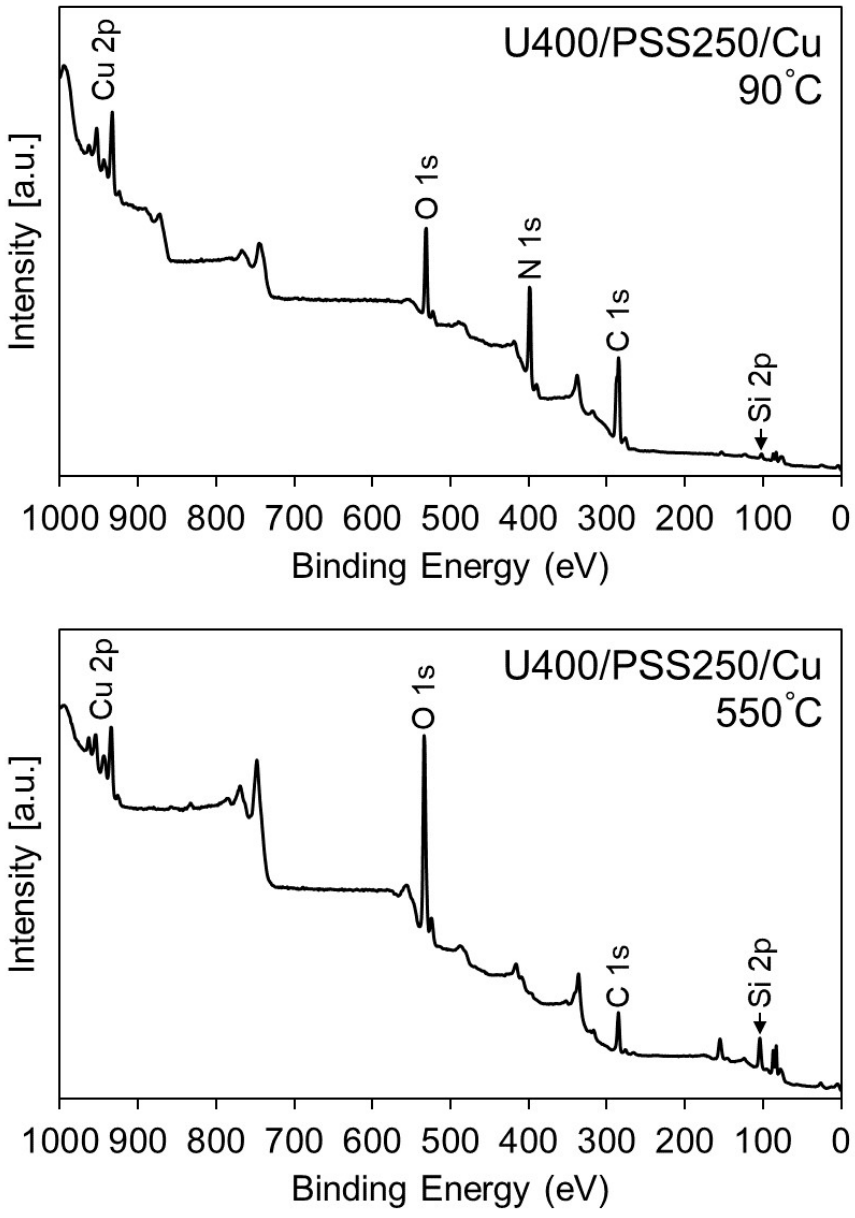

Fig. S6 XPS survey scan for U400/PSS250/Cu 90°C and U400/PSS250/Cu 550°C.

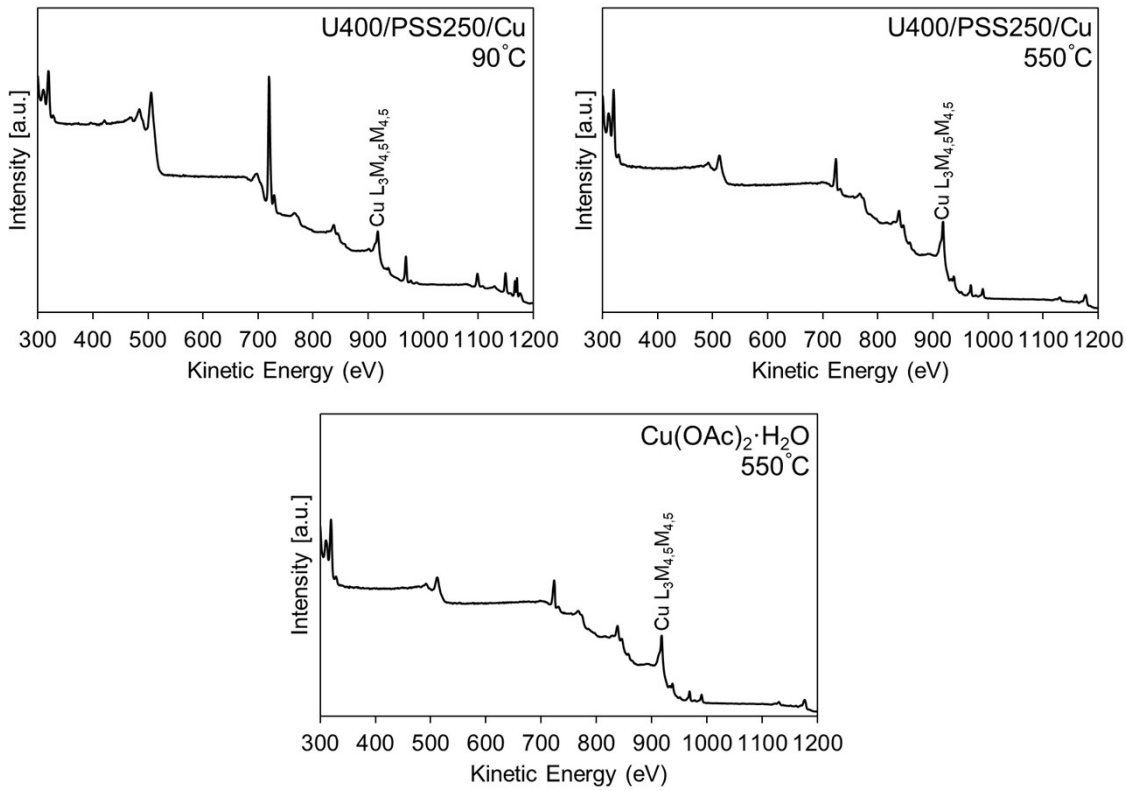

Fig. S7 XPS survey scan for U400/PSS250/Cu 90°C, U400/PSS250/Cu 550°C, and $Cu(OAc)_2 \cdot H_2O$ 550°C in kinetic energy scale.

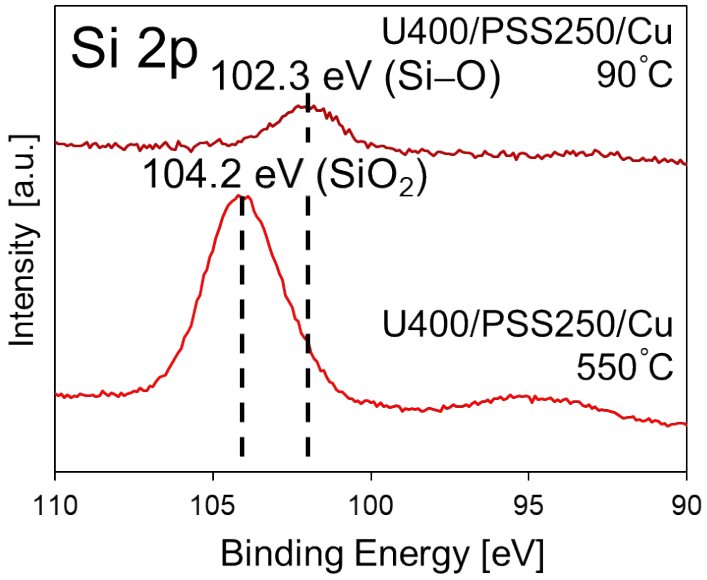

Fig. S8 High-resolution XPS spectra in Si 2p region for U400/PSS250/Cu 90°C and U400/PSS250/Cu 550°C.

Table S2 Calculated Auger parameters.

	Cu $2p_{3/2}$ photoelectron peak [eV]	Cu $L_3M_{4,5}M_{4,5}$ Auger peak [eV]	Auger parameter [eV]
U400/PSS250/Cu 90°C	933.04	915.44	1848.5
U400/PSS250/Cu 550°C	934.08	917.70	1851.8
$Cu(OAc)_2 \cdot H_2O$ 550°C	933.59	918.05	1851.6

Table S3 The element ratio of Si and Cu in U400/PSS250/Cu 550°C.

	1	2	3	4	5	
Si [at%]	43.81	44.41	38.32	46.58	46.77	
Cu [at%]	56.19	55.59	61.68	53.42	53.23	
	6	**7**	**8**	**9**	**10**	**Average**
Si [at%]	46.86	48.01	50.91	45.75	47.33	45.9
Cu [at%]	53.14	51.99	49.09	54.25	52.67	54.1

Table S4 The element ratio of Si and Cu in U400/PSS500/Cu 550°C.

	1	2	3	4	5	
Si [at%]	36.77	38.36	29.14	39.30	44.05	
Cu [at%]	63.23	61.64	70.86	60.70	55.95	
	6	**7**	**8**	**9**	**10**	**Average**
Si [at%]	34.01	30.60	29.61	45.96	45.46	37.3
Cu [at%]	65.99	69.40	70.39	54.04	54.54	62.7

Table S5 The element ratio of Si and Cu in U400/PSS1500/Cu 550°C.

	1	2	3	4	5	
Si [at%]	53.07	48.86	48.00	41.55	44.20	
Cu [at%]	46.93	51.14	52.00	58.45	55.80	
	6	**7**	**8**	**9**	**10**	**Average**
Si [at%]	42.88	50.68	53.35	47.46	49.10	47.9
Cu [at%]	57.12	49.32	46.65	52.54	50.90	52.1

Table S6 Experimental yields of U400/PSSx/Cu 550°C and theoretical yields of CuO and SiO_2.

Product name	Precursors (Before calcination 550°C) [mg]	Products (After calcination 550°C) [mg]	Experimental Yield [%]	Theoretical yield of CuO and SiO_2 [%]
U400/PSS250/Cu 550°C	987	115	11.7	15.5
U400/PSS500/Cu 550°C	1449	280	19.3	22.5
U400/PSS1500/Cu 550°C	1705	516	30.3	32.3

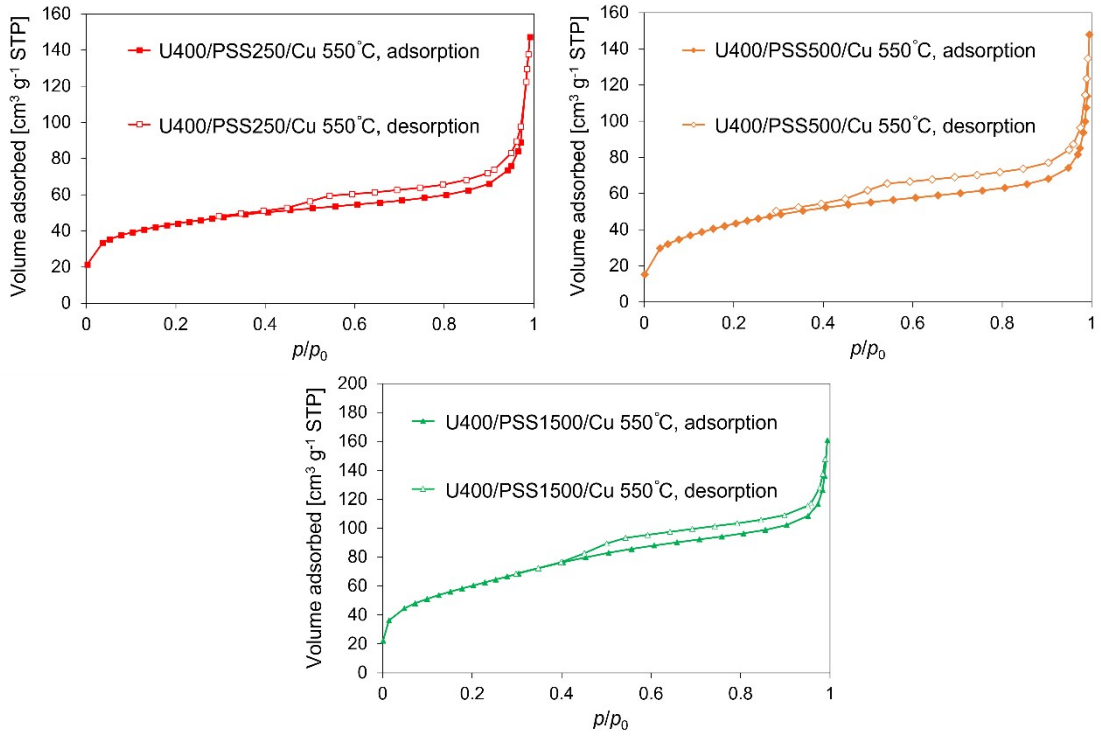

Fig. S9 N_2 adsorption–desorption isotherms of each U400/PSSx/Cu 550°C.

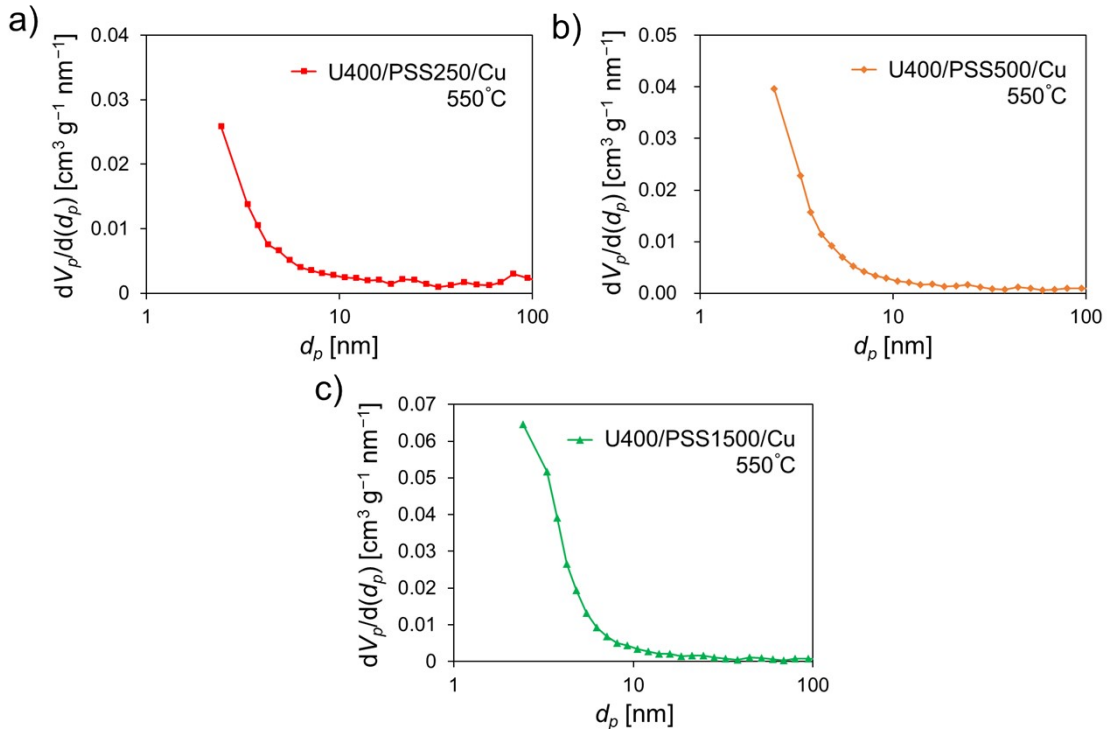

Fig. S10 BJH pore size distributions of a) U400/PSS250/Cu 550°C, b) U400/PSS500/Cu 550°C, and c) U400/PSS1500/Cu 550°C.

Table S7 Specific surface areas of each material.

	Specific surface area [m^2 g^{-1}]
U400/PSS250/Cu 550°C	157
U400/PSS500/Cu 550°C	153
U400/PSS1500/Cu 550°C	214
$Cu(OAc)_2 \cdot H_2O$ 550°C	1

Table S8 Comparative table from the literature in porosity.

	Method	Specific surface area [$m^2\ g^{-1}$]	Ref.
CuO nanochains	Wet chemical route using polyethylene glycol as a soft template	123.1	1
CuO nanosheets clusters	Hydrothermal method with/without surfactants	75.40, 95.31, 93.87	2
CuO hollow microspheres	Carbon spheres used as templates	74.81	3
Porous CuO	Calcination of metal–organic frameworks	69.57, 89.18	4
CuO ultrathin nanobelts	Wet chemical method combined with a fast calcination strategy	109.13	5
Mesoporous CuO dandelion Structures	Hydrothermal route	325	6
Porous CuO	Calcination process via the chemical solution deposition to prepare the copper oxalate precursor	165, 193, 295	7
CuO/SiO_2 composites	Solution exchange of wet silica gel (CuO content: 30 wt%)	158	8
Hollow CuO@SiO_2 spheres	Template method using Cu@C composite as a hard template (Cu content: 26 wt%)	85	9
Porous CuO–SiO_2 nanocomposites	Structure-directing synthesis via calcination	153, 157, 214	In this study

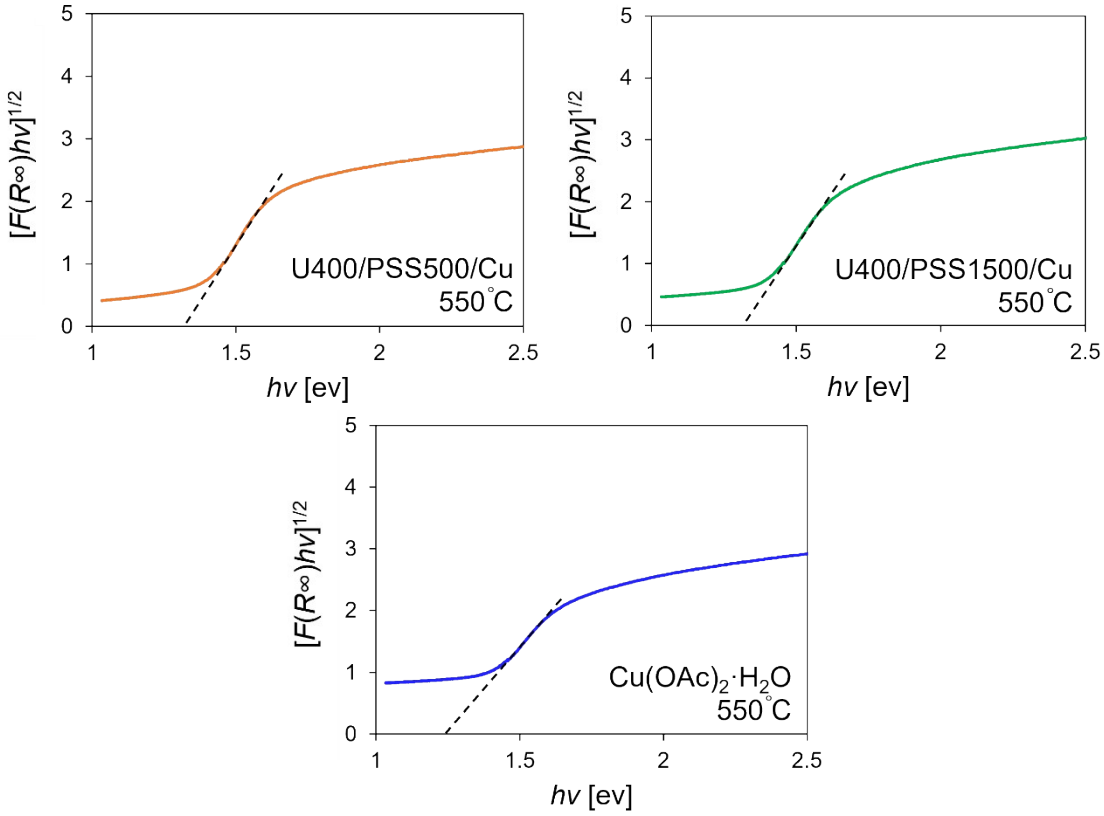

Fig. S11 Optical band gaps of U400/PSS500/Cu 550°C, U400/PSS1500/Cu 550°C, and $Cu(OAc)_2 \cdot H_2O$ 550°C determined with the plots of $[F(R\infty)h\nu]^{1/2}$ versus photon energy ($h\nu$).

Table S9 Comparative table from the literature in band gap.

	Band gap [eV]	Ref.
CuO–ZnO core–shell nanowire	1.5–1.6	10
CuO@TiO_2 heterostructure composite	2.35	11
CuO/$CuFe_2O_4$ nanocomposites	1.37–1.72	12
Core/shell nanoparticles of SiO_2@CuO	2.63–4.20	13
CuO/SiO_2 monolith	1.33	14
Porous CuO–SiO_2	1.3	In this study

nanocomposites

Table S10 The element ratio of Si and Cu in PSS/Cu 550°C.

	1	2	3	4	5	
Si [at%]	0	0	0	11.48	7.39	
Cu [at%]	100	100	100	88.52	92.61	
	6	**7**	**8**	**9**	**10**	**Average**
Si [at%]	0	0	6.61	10.06	4.77	4.03
Cu [at%]	100	100	93.39	89.94	95.23	95.97

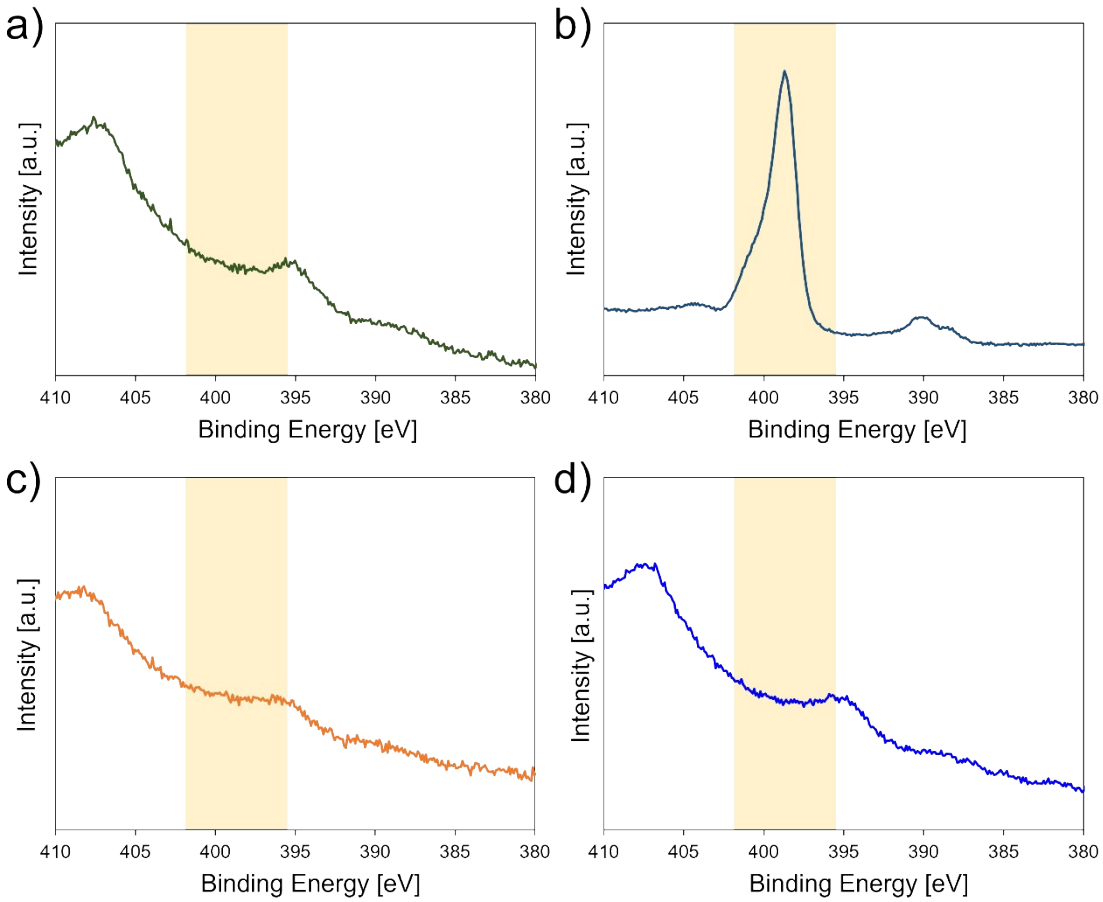

Fig. S12 High-resolution XPS spectra in the N 1s region for a) U400/Cu 550°C, b) U400/PSS 550°C, c) U400/PSS500/Cu 550°C, and d) the background ($Cu(OAc)_2 \cdot H_2O$ 550°C).

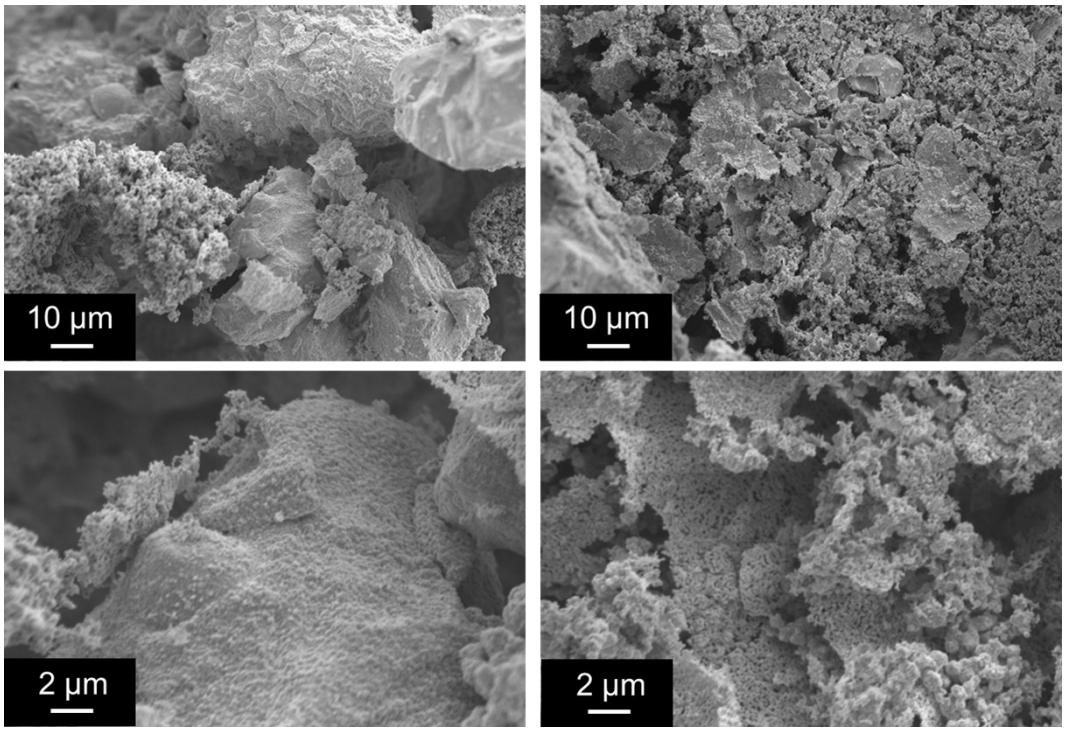

Fig. S13 SEM images of $Cu(OAc)_2 \cdot H_2O$ 550°C.

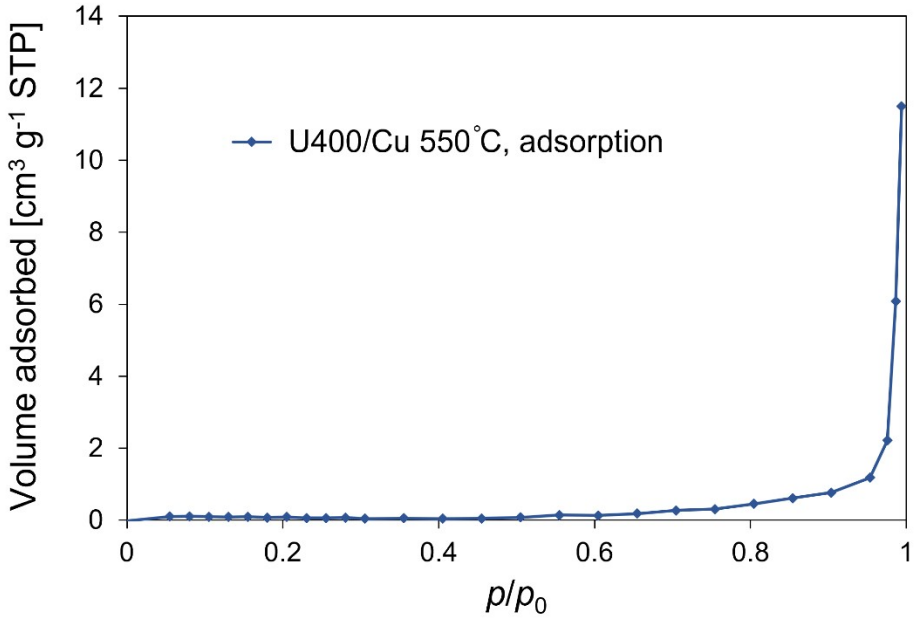

Fig. S14 The N_2 adsorption isotherm of U400/Cu 550°C.

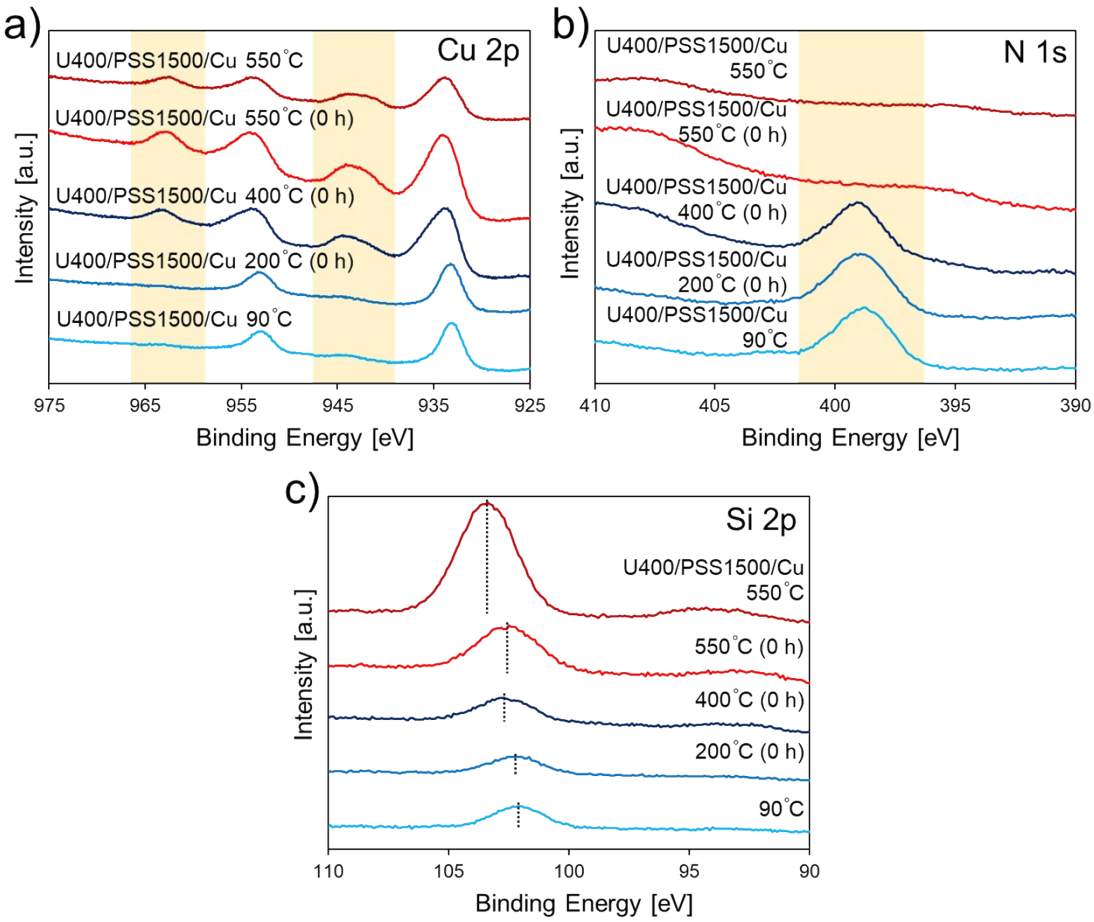

Fig. S15 High-resolution XPS spectra in a) Cu 2p region, b) N 1s region, and c) Si 2p region for U400/PSS1500/Cu 90°C and the samples obtained by calcinating U400/PSS1500/Cu 90°C at different conditions.

References

1. P. Wang, X.-X. Gou, S. Xin and F.-F. Cao, *New J. Chem.*, 2019, **43**, 6535–6539.
2. G. S. Gund, D. P. Dubal, D. S. Dhawale, S. S. Shinde and C. D. Lokhande, *RSC Adv.*, 2013, **3**, 24099–24107.
3. Q. Shao, X. Wang, Q. Liu, L. Wang, C. Kang, Q. Wang and S. Ge, *J. Nanosci. Nanotechnol.*, 2011, **11**, 10271–10277.
4. K. Kim, P. G. Choi, T. Itoh and Y. Masuda, *Adv. Mater. Interfaces*, 2021, **8**, 2100283.
5. Q. Wang, Y. Zhou, K. Zhang, Y. Yu, Q. Luo, S. Gao and Y. Xie, *J. Mater. Chem. A*, 2023, **11**, 8776–8782.
6. S. Manna, K. Das and S. K. De, *ACS Appl. Mater. Interfaces*, 2010, **2**, 1536–1542.
7. Z. Jia, L. Yue, Y. Zheng and Z. Xu, *Mater. Res. Bull.*, 2008, **43**, 2434–2440.
8. R. Takahashi, S. Sato, T. Sodesawa, M. Kato and S. Yoshida, *J. Sol–Gel Sci. Technol.*, 2000, **19**, 715–718.
9. X. Niu, T. Zhao, F. Yuan and Y. Zhu, *Sci. Rep.*, 2015, **5**, 9153.
10. A. Costas, C. Florica, N. Preda, C. Besleaga, A. Kuncser and I. Enculescu, *Sci. Rep.*, 2022, **12**, 6834.
11. H. Hamad, M. M. Elsenety, W. Sadik, A.-G. El-Demerdash, A. Nashed, A. Mostafa and S. Elyamny, *Sci. Rep.*, 2022, **12**, 2217.
12. M. M. Rashad, S. Soltan, A. A. Ramadan, M. F. Bekheet and D. A. Rayan, *Ceram. Int.*, 2015, **41**, 12237–12245.
13. Z. Rahimabadi, M. M. Bagheri-Mohagheghi and A. Shirpay, *J. Mater. Sci. Mater. Electron.*, 2022, **33**, 7765–7780.
14. S. Sharma and S. Basu, *Sep. Purif. Technol.*, 2021, **279**, 119759.